arXiv:1402.4290v2 [cond-mat.soft] 27 Feb 2014

# Soliton dynamics in a solid lubricant during sliding friction

Anna Vigentini,[1] Barbara Van Hattem,[1] Elena Diato,[1] Paolo Ponzellini,[1] Tommaso Meledina,[1] Andrea Vanossi,[2,3] Giuseppe Santoro,[3,2,4] Erio Tosatti,[3,2,4] and Nicola Manini[1,2,3]

[1] *Dipartimento di Fisica, Università degli Studi di Milano, Via Celoria 16, 20133 Milano, Italy*
[2] *CNR-IOM Democritos National Simulation Center, Via Bonomea 265, 34136 Trieste, Italy*
[3] *International School for Advanced Studies (SISSA), Via Bonomea 265, 34136 Trieste, Italy*
[4] *International Center for Theoretical Physics (ICTP), Strada Costiera 11, 34151 Trieste, Italy*

(Dated: March 3, 2014)

Recent highly idealized model studies of lubricated nanofriction for two crystalline sliding surfaces with an interposed thin solid crystalline lubricant layer showed that the overall relative velocity of the lubricant $v_{\rm lub}/v_{\rm slider}$ depends only on the ratio of the lattice spacings, and retains a strictly constant value even when system parameters are varied within a wide range. This peculiar "quantized" dynamical locking was understood as due to the sliding-induced motion of misfit dislocations, or soliton structures. So far, the practical relevance of this concept to realistic sliding three dimensional crystals has not been demonstrated. In this work, by means of classical molecular dynamics simulations and theoretical considerations, we realize a realistic three-dimensional crystal-lubricant-crystal geometry. Results show that the flux of lubricant particles associated with the advancing soliton lines gives rise here too to a quantized velocity ratio. Moreover, depending on the interface lattice spacing mismatch, both forward and backward quantized motion of the lubricant is predicted. The persistence under realistic conditions of the dynamically pinned state and quantized sliding is further investigated by varying sliding speed, temperature, load, and lubricant film thickness. The possibilities of experimental observation of quantized sliding are also discussed.

PACS numbers: 68.35.Af, 46.55.+d, 81.40.Pq, 61.72.Hh

## I. INTRODUCTION

The problem of boundary lubricated friction of two perfect sliding crystal surfaces is fascinating both from the fundamental point of view and for applications in the wider context of nanofriction.[1] Intriguing and unexpected behavior of the relative lubricant velocity have recently been reported in numerical simulations, depending on the "degree" of geometrical incommensurability defining the moving interface. The main nontrivial feature is the asymmetry in the sliding velocity of the intermediate lubricant sheet relative to the two substrates.[2–12]. Moreover, and even more strikingly, the lubricant mean velocity takes a constant, "quantized", value uniquely determined by the incommensurability ratios of the three spatial periodicities involved – the two sliders and the interposed solid lubricant – and is insensitive to other physical parameters of the model. The sliding steady state versus overall sliding velocity, as well as other parameters, is characterized by perfectly flat plateaus in the ratio of the time-averaged lubricant center of mass (c.m.) velocity to the externally imposed relative speed $v_{\rm ext}$ of the two sliders. This amounts to a kind of "dynamical incompressibility" or dynamic pinning, namely, identically null velocity response to perturbations or fluctuations trying to deflect the relative lubricant velocity away from its quantized value. The occurrence of this surprising regime of motion was ascribed to the intrinsic topological nature of this locked dynamics. This phenomenon, investigated in detail in rather idealized one-dimensional (1D) geometries[2–10], was explained by the grip exerted by one slider onto the topological solitons (called kinks or antikinks in one-dimension) that the embedded solid lubricant lattice forms with the other slider. The pinning of these solitons by the first slider causes their rigid dragging at the full sliding speed $v_{\rm ext}$. As a result the overall mean lubricant speed is a fixed ratio $w$ of the slider's speed, strictly determined by the soliton spatial density, a purely geometrical factor $|w| < 1$. Simulation evidence of this particular sliding regime was also confirmed for a less idealized 1+1-dimensional (1+1D) model of boundary lubrication[11,12], where Lennard-Jones (LJ) interacting atoms were allowed to move freely, parallel and perpendicularly to the sliding direction. Solitons formed in this case too, and their influence transmitted from one slider to the other across the lubricant film even when the thickness is as large as six atomic layers.

In this work, we simulate lubricated sliding in a fully 3D prototypical model. We again find that, under fairly general conditions, the lubricant slides relative to a fixed surface with a mean relative lubricant velocity component in the driving direction $w = v_{\rm c.m.\,x}/v_{\rm ext}$, which is "quantized" to a basically parameter-independent value $w = w_{\rm quant}$, much as was observed for the essentially 1D models. Confirming its soliton nature here too, we characterize the properties and limitations of the quantized-velocity dynamics in the 3D model, showing that the quantized sliding is robust against wide-range variations of different model parameters.

An intuitive and suggestive picture of the advancing solitons in the quantized state can be appreciated by the side view of the 3D geometry of Fig. 1. One can note the characteristic "caterpillar" motion executed by the lubricant particles in contact with the closest-matched

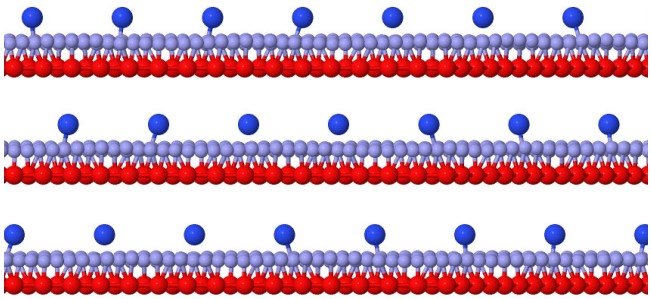

Figure 1: (Color online) Side view of the substrate-lubricant-substrate sandwich, with the static bottom substrate (red), the mobile lubricant atoms (light blue, smaller) and the top rigid slider, with much larger spacing (dark blue). Three successive time frames illustrate the "caterpillar" soliton motion driven by the rightward advancing top layer. Note the small vertical corrugations of the lubricant layer.

crystal surface. In the 3D geometry actually the soliton (Moiré) pattern is a 2D feature, which in general implies additional characteristics, such as mismatches induced by relative lattice rotation[13]. In this 3D study we will however restrict our investigation to mutually aligned incommensurate geometries, deferring the rotated cases to future work.

## II. THE MODEL

We represent the two confining 3D crystal surfaces by perfectly periodic 2D ($xy$) monolayers, rigidly arranged in close-packed triangular lattices representing, e.g. the (111) face of a cubic crystal. Between these two rigid planar sliders we insert $N_{\rm layer}$ layers of generally crystallized but mobile lubricant atoms, see Fig. 1. Each layer is composed of point-like classical particles of unit mass ($m = 1$). While the reciprocal intra-layer positions of top and bottom slider atoms are of course fixed, the atoms composing the lubricant film move freely under the action of pairwise (6,12) LJ interactions among one another and with the rigid atoms forming the top and the bottom surfaces. The standard LJ interaction

$$\phi_{\rm LJ}(r) = \varepsilon \left[ \left(\frac{\sigma}{r}\right)^{12} - 2\left(\frac{\sigma}{r}\right)^{6} \right] , \qquad (1)$$

is characterized by depth $\varepsilon$ and radius $r = \sigma$. We truncate the interaction at a cutoff radius $R_{\rm C} = 2.5\sigma$ and shift the 2-body potential energy to eliminate the energy discontinuity as follows:

$$\phi(r) = \begin{cases} \phi_{\rm LJ}(r) - \phi_{\rm LJ}(R_{\rm C}) & r \le R_{\rm C} \\ 0 & r > R_{\rm C} \end{cases} . \qquad (2)$$

The motion of the $j$-th lubricant particle is ruled by the equation of motion

$$\begin{aligned} m\ddot{\vec{r}}_j = &- \sum_{i_{\rm t}=1}^{N_{\rm t}} \frac{\partial}{\partial \vec{r}_j} \phi^{\rm t,p}(|\vec{r}_j - \vec{r}_{i_{\rm t}}|) + \\ &- \sum_{\substack{j'=1 \\ j'\neq j}}^{N_{\rm p}} \frac{\partial}{\partial \vec{r}_j} \phi^{\rm p,p}(|\vec{r}_j - \vec{r}_{j'}|) + \\ &- \sum_{i_{\rm b}=1}^{N_{\rm b}} \frac{\partial}{\partial \vec{r}_j} \phi^{\rm b,p}(|\vec{r}_j - \vec{r}_{i_{\rm b}}|) + \vec{f}_{{\rm damp}\,j} + \vec{f}_j(t) \,, \end{aligned} \qquad (3)$$

where $\vec{r}_j$ is the position of the $j$-th lubricant particle; $\vec{r}_{i_{\rm t}}$ and $\vec{r}_{i_{\rm b}}$ are the positions of the top and bottoms slider atoms, $N_{\rm b}$, $N_{\rm p}$ and $N_{\rm t}$ are the numbers of the bottom, lubricant and top particles, and $\phi^{\rm b,p}$, $\phi^{\rm p,p}$ and $\phi^{\rm t,p}$ are the truncated 2-body potential energies for the interactions between bottom-lubricant, lubricant-lubricant and top-lubricant particles, respectively, characterized by generally different $\sigma$ and $\varepsilon$ parameters, as specified below. $\vec{f}_{{\rm damp}\,j}$ and $\vec{f}_j(t)$ are a damping force and a random force respectively, used to implement a Langevin dynamics, as detailed below.

By convention, we select the bottom slider as our reference frame. The top slider is forced to move rigidly along $\hat{x}$ at a fixed horizontal velocity $\dot{r}^{\rm top}_{x_{i_{\rm t}}}(t) \equiv v_{\rm ext}$, under an external downward force $-F_{\rm load}\,\hat{z}$ applied to each particle in the slider. It also generally moves along the $\hat{y}$ and $\hat{z}$ axes (its inertia equals the total mass $N_{\rm t}$ of its atoms) under the interaction between its atoms and those of the lubricant film. For these $\hat{y}$ and $\hat{z}$ components, the motion of the top slider is described by

$$N_{\rm t} m \ddot{r}^{\rm top}_{y_{i_{\rm t}}}(t) = - \sum_{i'_{\rm t}=1}^{N_{\rm t}} \sum_{j=1}^{N_{\rm p}} \frac{\partial}{\partial r_y} \phi^{\rm t,p}(|\vec{r}_{i'_{\rm t}} - \vec{r}_j|) + F_{{\rm th}\,y} \qquad (4)$$

$$\begin{aligned} N_{\rm t} m \ddot{r}^{\rm top}_{z_{i_{\rm t}}}(t) = &- \sum_{i'_{\rm t}=1}^{N_{\rm t}} \sum_{j=1}^{N_{\rm p}} \frac{\partial}{\partial r_z} \phi^{\rm t,p}(|\vec{r}_{i'_{\rm t}} - \vec{r}_j|) \\ &+ F_{{\rm th}\,z} - N_{\rm t} F_{\rm load} \,, \end{aligned} \qquad (5)$$

where the components of the thermostat force $\vec{F}_{\rm th}$ are discussed below. As all equations for $r^{\rm top}_{y/z_{i_{\rm t}}}$ are the same, irrespective of $i_{\rm t}$, in practice their solution only differs by a translation $\vec{r}^{\rm top}_{i_{\rm t}} \equiv \vec{r}^{\rm top} + \vec{r}^{\rm init}_{i_{\rm t}}$ (where $\vec{r}^{\rm init}_{i_{\rm t}}$ are the initial positions of the rigid top 2D lattice), so that equations for $r^{\rm top}_y$ and $r^{\rm top}_z$ only are integrated.

### A. Frictional work and thermostat

The total force needed to maintain the top slider at the fixed velocity $v_{\rm ext}$ compensates exactly the total force which the lubricant exerts on the top slider itself:

$$F_{\rm frict} = \sum_{i'_{\rm t}=1}^{N_{\rm t}} \sum_{j=1}^{N_{\rm p}} \frac{\partial}{\partial r_x} \phi^{\rm t,p}(|\vec{r}_{i'_{\rm t}} - \vec{r}_j|) - F_{{\rm th}\,x} \,. \qquad (6)$$

The work of this frictional force

$$W_{\rm frict} = \int_0^\tau F_{\rm frict} v_{\rm ext}\, dt = v_{\rm ext} \int_0^\tau F_{\rm frict}\, dt = \tau v_{\rm ext} \bar{F}_{\rm frict} \tag{7}$$

represents the total Joule heat that the advancing top layer pumps into the mechanical system over a time interval $\tau$.

To remove this Joule heat, to reach a steady state, and to control the rise of lubricant temperature in this driven system, we use a standard implementation of the Langevin dynamics, Eq. (3), including a phenomenological viscous damping term, plus a Gaussian random force $\vec{f}_j(t)$. To avoid biasing the lubricant motion by privileging either the bottom or the top reference frame, the damping force includes two contributions representing the energy dissipation into both sliders

$$\vec{f}_{{\rm damp}\,j} = -\eta \dot{\vec{r}}_j - \eta(\dot{\vec{r}}_j - \dot{\vec{r}}_{\rm t})\,. \tag{8}$$

Taking into account this twofold contribution to dissipation, the zero-average Gaussian random forces satisfy

$$\langle f_{j\beta}(t) f_{j'\beta'}(t')\rangle = 4\eta k_{\rm B} T \delta_{jj'}\delta_{\beta\beta'}\delta(t-t')\,, \tag{9}$$

(with $\beta, \beta' = x, y, z$ components), so that in a non-sliding regime ($v_{\rm ext} = 0$) the Langevin thermostat leads to a stationary state characterized by standard Boltzmann equilibrium average kinetic energy of the lubricant:

$$\langle E_{\rm k}\rangle = 3N_{\rm p}\frac{1}{2}k_{\rm B}T\,. \tag{10}$$

The damping force contribution representing the energy dissipation into the top slider requires a force balance (Newton's third law) term in Eqs. (4) and (5) for the top layer:

$$\vec{F}_{\rm th} = \eta \sum_i^{N_{\rm p}} (\dot{\vec{r}}_i - \dot{\vec{r}}_{\rm t}) = \eta N_{\rm p}(\vec{v}_{\rm c.m.} - \dot{\vec{r}}_{\rm t})\,. \tag{11}$$

While the $\hat{y}$ and $\hat{z}$ components of this additional term have a real influence on the top motion through Eqs. (4) and (5), of course its $\hat{x}$ component does not. It only contributes to the external force $F_{\rm frict}$ required to maintain the top velocity $\hat{x}$ component constant and equal to $v_{\rm ext}$, with the last term in Eq. (6).

As long as the value of $\eta$ is so small[14] that it produces an underdamped dynamics, the thermostat perturbs the atomistic dynamics only marginally. Under this condition, the Langevin method represents a simple but numerically stable and effective phenomenological approach to describe energy dissipation into the substrates occurring e.g., through the excitation of phonons and (in the case of metals) of electron-hole pairs, etc. We verified that all qualitative results are insensitive to the value of $\eta$ (as long as it is small enough), although quantitative issues such as the precise boundary of the quantized sliding regime do depend on $\eta$. More refined methods were proposed and adopted in similar simulations[15–22] but to investigate the occurrence and main properties of the quantized sliding phenomenon, a simple Langevin approach to power dissipation is sufficient and appropriate.

| Physical quantity | Natural units | Typical value |
|---|---|---|
| length | $a_{\rm b}$ | 0.2 nm |
| mass | $m$ | 50 a.m.u.$\simeq 8.3\times10^{-26}$ kg |
| energy | $\varepsilon_{\rm pp}$ | 1 eV $\simeq 1.6\times10^{-19}$ J |
| time | $a_{\rm b}\, m^{1/2}\varepsilon_{\rm pp}^{-1/2}$ | 0.14 ps |
| velocity $v$ | $m^{-1/2}\varepsilon_{\rm pp}^{1/2}$ | 1400 m/s |
| force | $a_{\rm b}^{-1}\,\varepsilon_{\rm pp}$ | 0.8 nN |

Table I: Natural units for several mechanical quantities in a system where length, mass and energy are measured in units of $a_{\rm b}$, $m$, $\varepsilon$. Typical physical values are also indicated.

### B. Length scales and units

The sliding system involves three generally different solids, two sliders and a lubricant, which in their crystalline state are characterized by generally different lattice spacings: $a_{\rm p}$, $a_{\rm t}$, and $a_{\rm b}$. For the particle-particle interaction inside the lubricant we take the LJ radius $\sigma_{\rm pp} = 1.01 a_{\rm p}$ so as to compensate approximately first-neighbor repulsion with second- and third-neighbor attraction. Interactions within each of the rigid sliders are of course not needed. However, one could still introduce them for convenience with radii $\sigma_{\rm tt} = a_{\rm t}$ and $\sigma_{\rm bb} = a_{\rm b}$, and fix slider-lubricant interaction radii $\sigma_{\rm tp}$ and $\sigma_{\rm bp}$ e.g. by means of the Lorentz-Berthelot mixing rules[23]:

$$\sigma_{\rm tp} = \frac{1}{2}(\sigma_{\rm tt} + \sigma_{\rm pp})\,, \quad \sigma_{\rm bp} = \frac{1}{2}(\sigma_{\rm bb} + \sigma_{\rm pp})\,. \tag{12}$$

In practice however we fix the radii according to $\sigma_{\rm tp} = \sigma_{\rm bp} = 1.02 a_{\rm b}$, and for simplicity, we fix the same interaction energy $\varepsilon_{\rm tp} = \varepsilon_{\rm pp} = \varepsilon_{\rm bp} = \varepsilon$ for all pairwise coupling terms, unless otherwise noted.

We consider a set of "natural" units in terms of $\varepsilon$ (energy), $a_{\rm b}$ (length), and $m$ (mass). All quantities are then expressed as dimensionless numbers. To obtain a physical quantity in its explicit dimensional form, one should multiply its simulated numerical value by the corresponding natural units listed in Table I.

The spacings $a_{\rm t}$, $a_{\rm p}$, and $a_{\rm b}$, and the angles of relative rotation, define the initial conditions for the sliders and the lubricant lattices. Each atomic layer is initially a perfect 2D triangular lattice. We stack complete layers, realizing an fcc crystalline film of lubricant as it would be at low temperature. The initial vertical separation between successive lubricant layers is of the order of $\sqrt{2/3}a_{\rm p}$.

The three different spacings $a_{\rm t}$, $a_{\rm b}$ and $a_{\rm p}$ give rise to two independent ratios affecting the 2D lattice mismatches:

$$r_{\rm t} = \frac{a_{\rm t}}{a_{\rm p}}\,, \quad r_{\rm b} = \frac{a_{\rm b}}{a_{\rm p}}\,. \tag{13}$$

We perform the numerical integration of Eqs. (3), (4) and (5) by means of an adaptive fourth-order Runge-Kutta-Fehlberg method, when $T = 0$, or, for finite $T$, a 6-

steps Runge-Kutta algorithm involving Langevin random forces, Eq. (9).

### C. Boundary conditions

In order to explore with ease a large number of different configurations and to follow their evolution long enough for the top and lubricant to advance by several lattice spacings, our simulations involve a number of lubricant atoms $N_{\rm p} \lesssim 10^3$, which is exceedingly small compared to those involved in a realistic sliding interface (easily of the order of $10^7$ in a $\mu$m$^2$). To alleviate the effect of finite size and impose precise lattice-spacing ratios, we use periodic boundary conditions (PBC) in the $xy$ plane: the particles are enclosed in a supercell generated by two vectors $\vec{a}_i^{\rm cell}$ of length $L$, replicated infinitely by means of rigid translations. Each particle $j$ in the box interacts not just with the other particles $j'$ in the supercell, but also with their translated images in the nearest neighboring cells by means of a standard minimum-image algorithm[23]. In the third ($\hat{z}$) direction, the lubricant is of course confined by top and bottom sliders. In the simple case in which the crystalline directions of the bottom, lubricant, and top lattices are parallel, it is straightforward to construct the appropriate supercell, whose side $L$ is an integer multiple (e.g. the smallest multiple) of all three 2D lattice spacings, which have therefore to be taken mutually commensurate. For example, for $a_{\rm b} = 1$, $a_{\rm p} = 25/29$, $a_{\rm t} = 25/4$, the smallest supercell is obtained by taking $L = 25$.

### D. The coverage ratio

The quantized velocity state was interpreted in 1D as the dynamical pinning of the periodic soliton pattern on the comparably long-wavelength corrugation potential produced by the top substrate[2,9]. Isomorphic to a static depinning transition (the role of particles now taken by the moving kinks of the lubricant-substrate interface), although different in nature, this pinning should be particularly robust for perfect one-to-one commensurate matching of the inter-soliton spacing $a_{\rm sol}$ and the top-slider lattice spacing $a_{\rm t}$,[9] a condition where the soliton dragging should be especially effective in producing the quantized state.

Whenever the top lattice and the soliton pattern are aligned along the same crystalline directions, it makes sense to define a length ratio

$$\Theta = \sqrt{\frac{N_{\rm sol}}{N_{\rm t}}} = \frac{a_{\rm t}}{a_{\rm sol}}\,, \qquad (14)$$

defining a "coverage", and whose actual value depends on the spacing of solitons $a_{\rm sol}$. The latter in turn is tuned by the geometric mismatch condition between the lubricant and bottom layers, as detailed in Sect. III A.

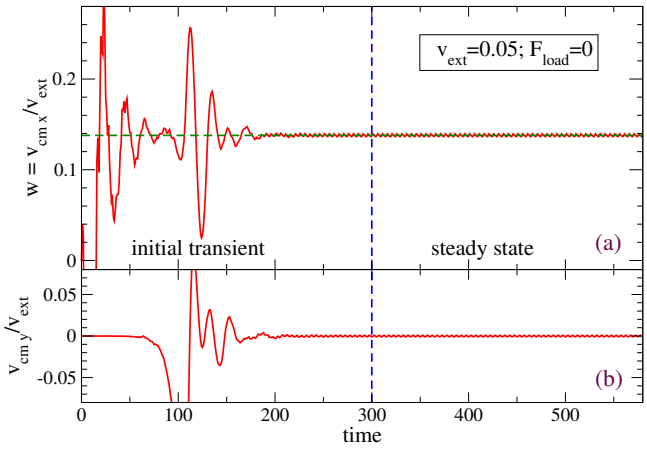


Figure 2: (Color online) A typical approach to the steady state for the $N_{\rm layer} = 1$ model represented in Fig. 3, with unrotated layers characterized by $a_{\rm t} = 25/4 = 6.25$, $a_{\rm p} = 25/29$, $a_{\rm b} = 1$. (a) Average lubricant velocity component in the driving direction, $w = v_{\rm c.m.\,x}/v_{\rm ext}$ (normalized by the top externally-fixed speed), as a function of time. After an initial transient, $w$ starts to fluctuate around the value predicted by Eq. (24): $w_{\rm quant} = 4/29 \simeq 0.1379$, marked by the horizontal dashed line. (b) The transverse ($y$) component of $\vec{v}_{\rm c.m.}$ stabilizes to 0 after the transient. The simulation is carried out with $F_{\rm load} = 0$, $T = 0$, $v_{\rm ext} = 0.05$. The transient detail depends on several physical quantities, including the initial configuration, the top speed $v_{\rm ext}$, temperature $T$, and the dissipation coefficient $\eta$. In contrast, the final value $w$ in the quantized-sliding state is completely insensitive to these details, but only depends on the lattice mismatch.

For most of the simulations described in the following we have selected an appropriate $r_{\rm b}$ to obtain $\Theta = 1$. However, as discussed later, we also investigated the quantized sliding for the less specific geometrical configuration when $r_{\rm b}$ is such that $\Theta$ deviates from unity.

## III. RESULTS

A simulation will represent the steady dynamical state of the system provided (i) that the simulation time is much longer than the relaxation times of all quantities of interest and (ii) that it yields a sufficiently long sampling of fluctuations to obtain accurate time averages in the dynamical steady state. In all our calculations we discard an initial transient, extending usually for a comparably long time (100 to 1000 time units), related to the poor damping produced by the relatively weakly coupled thermostat ($\eta = 0.05$). Figure 2 illustrates a typical transient regime for the lubricant center-mass velocity. Over the ensuing steady running state, we evaluate the time-averages of physical quantities. Whenever the quantities to be averaged happen to fluctuate periodically, we minimize systematic errors by evaluating these averages over one or several periods.

When we run simulations with different $v_{\rm ext}$, we set

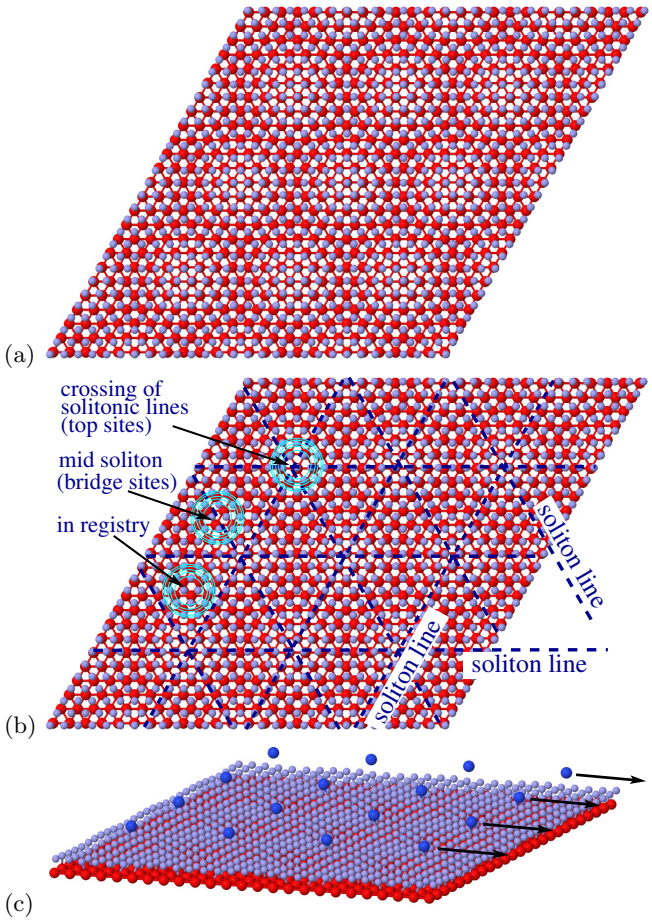


Figure 3: (Color online) A snapshot of the sliding steady state of the simulation of Fig. 2, representing the atoms inside one PBC-repeated supercell, in the same color convention as Fig. 1. The bottom slider and the lubricant are aligned with a lattice spacing mismatch of $r_{\rm b} = a_{\rm b}/a_{\rm p} = 29/25 = 1.16$, producing a clear soliton pattern. (a) Top view of a lattice-mismatched configuration, where only the bottom slider atoms (larger, red) and lubricant atoms (smaller, light blue) are shown. (b) Same top view as (a), with marked soliton lines and their crossings (top-site lubricant atoms), and in-registry regions (hollow-site lubricant atoms). These regions form a loose triangular lattice of spacing $a_{\rm sol} = 25/4 a_{\rm b} = 6.25\, a_{\rm b}$. (c) Lateral perspective view, with the advancing top layer (dark blue particles) spaced by $a_{\rm t} = a_{\rm sol}$ also included.

the total evolution time of each simulation $t_{\rm calc}$ by fixing the product $t_{\rm calc}\, v_{\rm ext}$, so that in a simulation the top slider advances by the same distance. We take at least $v_{\rm ext}\, t_{\rm calc} = 10$ length units for each simulation, and we also include a condition that $t_{\rm calc}$ never decreases under 100 time units, which is usually sufficient because when $v_{\rm ext}$ is changed in small steps transients are shorter than the one illustrated in Fig. 2. For moderate speeds $v_{\rm ext} \lesssim 1$, this choice allows the system enough time for all initial transient stresses induced by a changed $v_{\rm ext}$ to relax, and for a steady sliding state to ensue.

Guided by the lesson learnt in earlier 1D models[2,9] – solitons formed in the lubricant by one slider are docked and dragged by the other slider – we adopt a geometry of near-commensuration of the lubricant spacing to that of the bottom slider, with $r_{\rm b}$ not far from unity, and $r_{\rm t}$ far away from unity and closer instead to commensurate with the soliton lattice. Figure 3 displays a configuration of this kind, which we adopt as a prototype in the present paper.

### A. Quantized lubricant sliding

Simulations show that in most cases the lubricant slides relative to the bottom substrate with a relative mean lubricant velocity component in the driving direction $w = v_{\rm c.m.\,x}/v_{\rm ext}$ giving rise to a plateau $w = w_{\rm quant}$ which is essentially parameter-independent, that is "quantized" as in the the more idealized models studied in the past. We ran several batches of MD simulations to characterize the properties and boundaries of this plateau of quantized-velocity dynamics in the 3D model. To evaluate the dragging of solitons and the ensuing velocity-quantization phenomenon in 3D, for each lubricant layer we need to compute the mean flux $\bar\Phi_{\rm p}$ of lubricant particles crossing a line of length $L_y$ transverse to the pulling direction. By dividing $\bar\Phi_{\rm p}$ by a hypothetical flux $\bar\Phi_{\rm p}^{v_{\rm ext}}$ of lubricant particles all moving across the $L_y$ line at speed $v_{\rm ext}$, we obtain

$$w \equiv \frac{v_{\rm c.m.\,x}}{v_{\rm ext}} \equiv \frac{\bar\Phi_{\rm p}}{\bar\Phi_{\rm p}^{v_{\rm ext}}}\,. \tag{15}$$

Firstly, we evaluate the length $\delta_{\rm sol}$ of a single soliton line that crosses our reference line $L_y$ in a time $\tau$, while advancing perpendicularly to its own elongation

$$\delta_{\rm sol} = v\,\tau\,\frac{\cos\nu}{\sin\nu} \tag{16}$$

where $\nu$ is the angle formed by the soliton line with the $L_y$ direction, also equaling the angle that the advancement direction makes with the pulling direction, see Fig. 4. We then evaluate the mean length of soliton lines crossing $L_y$ in a unit time for a train of parallel soliton lines separated by a mutual distance $d$:

$$\bar V = \frac{\delta_{\rm sol}}{\tau}\,\frac{L_y \sin\nu/v}{d/v} = v\,\frac{\cos\nu}{\sin\nu}\,\frac{L_y\sin\nu}{d} = \frac{L_y}{d}\,v\,\cos\nu\,, \tag{17}$$

where $d/v$ represents the time between two successive solitons starting to cross $L_y$, and $L_y \sin\nu/v$ the time it takes for one such crossing to occur.

We first apply this general result to the case of a soliton pattern formed by a lattice-spacing mismatch between two aligned triangular lattices. In terms of the spacing $a_{\rm sol}$ of the lattice of soliton-crossing areas, see Fig. 3b, successive soliton lines are separated by $d = \frac{\sqrt{3}}{2}\, a_{\rm sol}$. The soliton spacing in the aligned case is given[24] by the 1D geometric mismatch condition

$$a_{\rm sol}^{-1} = a_{\rm p}^{-1} - a_{\rm b}^{-1}\,. \tag{18}$$

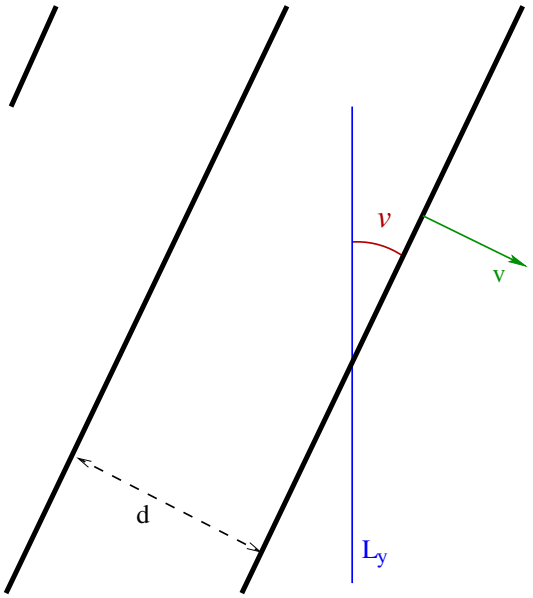


Figure 4: (Color online) A train of lines, spaced by a distance $d$, moves perpendicular to their direction at speed $v$ and crosses a segment of length $L_y$ at an angle $\nu$. This construction allows us to evaluate the length of line crossing the segment per unit time, Eq. (17).

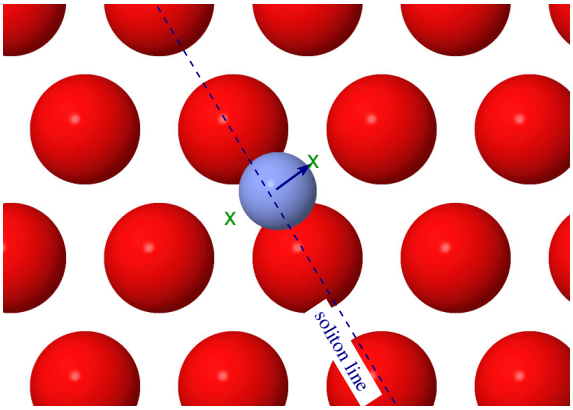


Figure 5: (Color online) A typical bridge atom along a soliton line (dashed line) moves from one hollow site to the next (green crosses), thus advancing perpendicularly to the soliton line.

A soliton line can only advance perpendicularly to itself, because the soliton-forming atoms stand locally at bridge sites relative to the bottom surface: Each atom is forced to cross the saddle-point energy barrier between highly-coordinated hollow sites moving in the energetically most favorable direction, which is perpendicular to the soliton line, see Fig. 5. The soliton intersections are dragged forward by the top layer moving at speed $v_{\rm ext}$.

This advancement is realized when each one of the soliton lines advances perpendicularly to itself at a speed $v = v_{\rm ext}\,\cos\nu$, namely a speed scaled by the angle that each line forms with the dragging direction. In the simplest case of unrotated lattices, see Fig. 6a, of the three soliton families, the one labeled 3 is horizontal, namely perpendicular to $L_y$, thus it does not contribute to the rightward sliding of the lubricant ($\nu = \pi/2$, thus $v = 0$). The two other families of solitons, labeled 1 and 2, both contribute a speed reduced by a factor $\cos\nu = \cos(\pi/6)$.

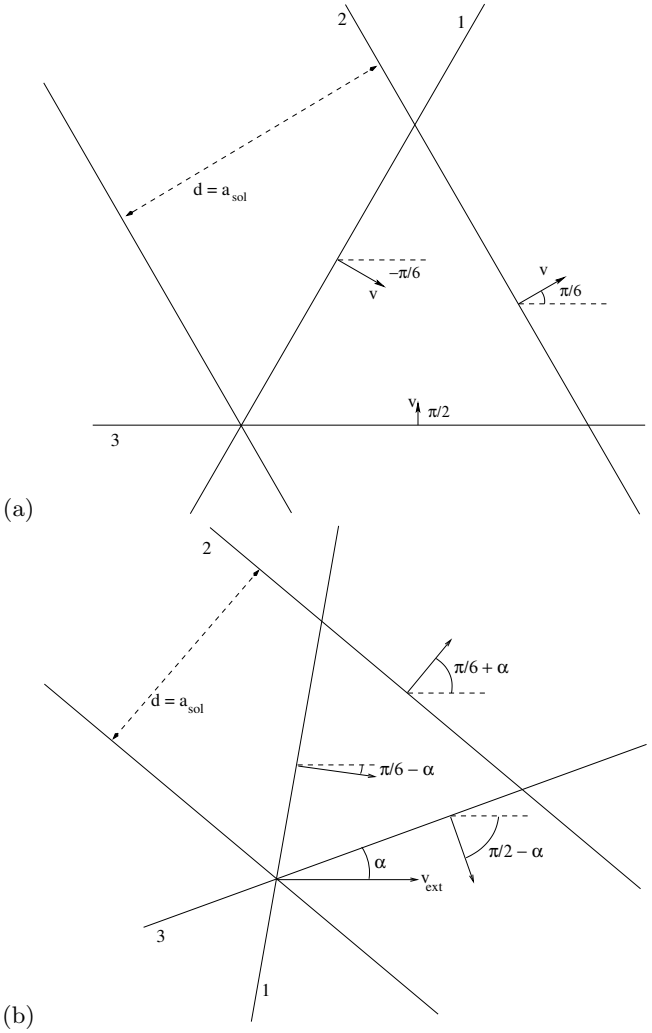


Figure 6: The geometry of a triangular lattice of soliton lines moving perpendicular to their direction at a speed $v$. (a) The case where the lines of type 3 are parallel to the dragging direction $\hat{x}$. (b) The case characterized by an overall rotation by $\alpha$ relative to the dragging direction $\hat{x}$.

Using Eq. (17), we evaluate the total speed of soliton lines crossing $L_y$ in this unrotated case, obtaining

$$\bar{V}_1 = \frac{L_y v_{\rm ext}\cos\frac{\pi}{6}\cos\frac{\pi}{6}}{a_{\rm sol}\sqrt{3}/2} = \frac{2L_y v_{\rm ext}}{\sqrt{3}a_{\rm sol}}\cos^2\frac{\pi}{6} \quad (19)$$

$$\bar{V}_2 = \bar{V}_1 \quad (20)$$

$$V_{\rm tot} = \bar{V}_1 + \bar{V}_2 = \frac{\sqrt{3}L_y v_{\rm ext}}{a_{\rm sol}}\,, \quad (21)$$

where $V_{\rm tot}$ includes contributions from all advancing soliton lines.

As a next step, we evaluate the flux of mobile particles associated with the advancing soliton lines. Recalling Fig. 3b, we observe that: (i) in-registry particles in between solitons do not contribute to sliding, as they are trapped in individual minima of the corrugation potential; (ii) a soliton line represents a single line of extra particles; (iii) as the soliton lines are parallel to the crystal principal directions, the line density of such extra particles along a soliton line is simply the reciprocal lattice spacing of the lubricant, $a_{\rm p}^{-1}$; (iv) one half of each soliton is composed of particles in the region in between soliton-crossing areas (bridge overlayer sites), which belong uniquely to that soliton, while the other half particles, those in the soliton crossing region (top sites), are shared by three solitons, thus the effective mean line density of mobile soliton particles is $\frac{1}{2}\times(1+\frac{1}{3})a_{\rm p}^{-1}=\frac{2}{3}a_{\rm p}^{-1}$. By multiplying this atomic linear density by $V_{\rm tot}$, we obtain the total flux of particles crossing $L_y$ per unit time, due to soliton advancement

$$\bar{\Phi}_{\rm p}=\frac{2L_y v_{\rm ext}}{\sqrt{3}\,a_{\rm p}a_{\rm sol}}\,. \tag{22}$$

We can now evaluate the dimensionless ratio of Eq. (15):

$$w=\frac{\bar{\Phi}_{\rm p}}{\bar{\Phi}_{\rm p}^{v_{\rm ext}}}=\frac{\frac{2L_y v_{\rm ext}}{\sqrt{3}\,a_{\rm p}a_{\rm sol}}}{\frac{L_y v_{\rm ext}}{\sqrt{3}\,a_{\rm p}^2/2}}=\frac{a_{\rm p}}{a_{\rm sol}}\,. \tag{23}$$

This expression is independent not just of $L_y$ but also of $v_{\rm ext}$, and it is a purely geometric function of the crystal lattice spacings which we can make explicit using Eq. (18) for $a_{\rm sol}$:

$$w=a_{\rm p}\left(\frac{1}{a_{\rm p}}-\frac{1}{a_{\rm b}}\right)=1-\frac{a_{\rm p}}{a_{\rm b}}=1-\frac{1}{r_{\rm b}}\equiv w_{\rm quant}\,. \tag{24}$$

This formula coincides with the 1D result[9] and matches the outcome of simulations as discussed in the next section.

In the case of a rigid overall rotation by a common angle $\alpha$, we apply the same theory, but we need to re-evaluate the speed of soliton lines crossing a line $L_y$ directed perpendicularly to the dragging direction $\hat{x}$. Using Eq. (17), we evaluate the crossing speed of the three families of parallel soliton lines shown in Fig. 6b:

$$\begin{aligned}
\bar{V}_1&=\frac{L_y\,v_{\rm ext}}{a_{\rm sol}\frac{\sqrt{3}}{2}}\cos^2\left(\frac{\pi}{6}-\alpha\right)\\
\bar{V}_2&=\frac{L_y\,v_{\rm ext}}{a_{\rm sol}\frac{\sqrt{3}}{2}}\cos^2\left(\frac{\pi}{6}+\alpha\right)\\
\bar{V}_3&=\frac{L_y\,v_{\rm ext}}{a_{\rm sol}\frac{\sqrt{3}}{2}}\cos^2\left(\frac{\pi}{2}-\alpha\right)\,.
\end{aligned} \tag{25}$$

By summing these three contributions, we obtain

$$\begin{aligned}
V_{\rm tot}&=\bar{V}_1+\bar{V}_2+\bar{V}_3 \qquad (26)\\
&=\frac{L_y\,v_{\rm ext}}{a_{\rm sol}\frac{\sqrt{3}}{2}}\left[\frac{3}{2}\cos^2\alpha+\frac{3}{2}\sin^2\alpha\right]=\frac{\sqrt{3}L_y v_{\rm ext}}{a_{\rm sol}}\,,
\end{aligned}$$

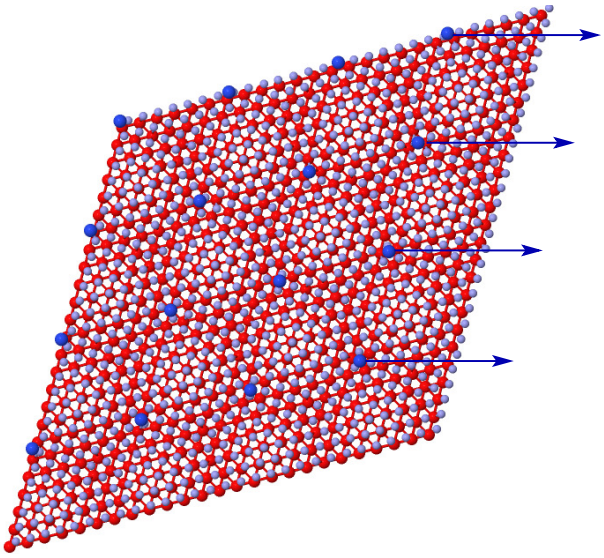

Figure 7: (Color online) Top view of the same model as in Fig. 3, but rotated rigidly by an angle $\alpha=\pi/12$ with respect to the original orientation. The top layer is still driven in the same horizontal direction $\hat{x}$ highlighted by arrows.

which coincides with the unrotated result, Eq. (21). As also the particle density along the soliton lines is the same, we obtain the same particle flux, as given by Eq. (24). We conclude that an overall rotation produces no change in the quantized sliding state, consistently with the fundamental isotropy of the triangular soliton net.

### B. Dragging solitons: forward lubricant motion

Zero-temperature MD simulations confirm the phenomenon of perfect velocity quantization in both the unrotated and the rigidly rotated case. As an example, the unrotated single-layer case of the model of Fig. 3 is characterized by $a_{\rm b}=25/29$, thus $r_{\rm b}=29/25$ and $a_{\rm sol}=29/4$: this indicates that we cross 4 soliton lines every 29 lubricant particles in each 2D-crystal high-symmetry direction. The choice $r_{\rm t}=a_{\rm sol}$ guarantees that for each one of these soliton lines, a line of top atoms is there to grab it. Figure 2a compares the instantaneous center-mass lubricant speed to the predicted quantized value of Eq. (24): after the initial transient, the resulting $v_{{\rm c.m.}\,x}$ makes a tiny oscillation around $w_{\rm quant}=4/29\simeq 0.1379$. This value of $r_{\rm b}$ is not to be considered in any way special: we find perfect quantized sliding for many other values of $r_{\rm b}$.

Likewise, by rotating rigidly the model of Fig. 3 e.g. by an angle $\alpha=\pi/12$, we obtain the geometry sketched in Fig. 7. When we pull the top slider along the same horizontal direction $\hat{x}$, we obtain the time evolution of the center of mass displayed in Fig. 8. Again, this velocity oscillates periodically around to the same relative value $w_{\rm quant}$, as predicted by Eq. (24), but with a different oscillation pattern. The longer period and larger oscillation

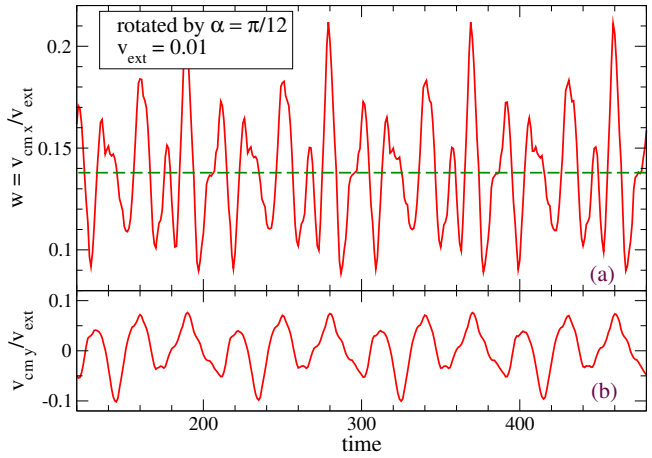


Figure 8: (Color online) (a) $\hat{x}$ and (b) $\hat{y}$ components of the lubricant center-mass velocity divided by the driving speed, $v_{\rm ext} = 0.01$, as a function of time for the rotated model of Fig. 7. The time-averaged center-mass $\hat{x}$ component coincides with the one obtained for the unrotated model, Fig. 2, and matches the quantized formula (24), dashed line. The amplitude and period of the fluctuations of $w$ around $w_{\rm quant}$ are both substantially larger than in the unrotated case, Fig. 2. The average $v_{\rm c.m.\,y}$ is consistent with the lubricant moving at an average angle of 1.1° with the $\hat{x}$ driving direction.

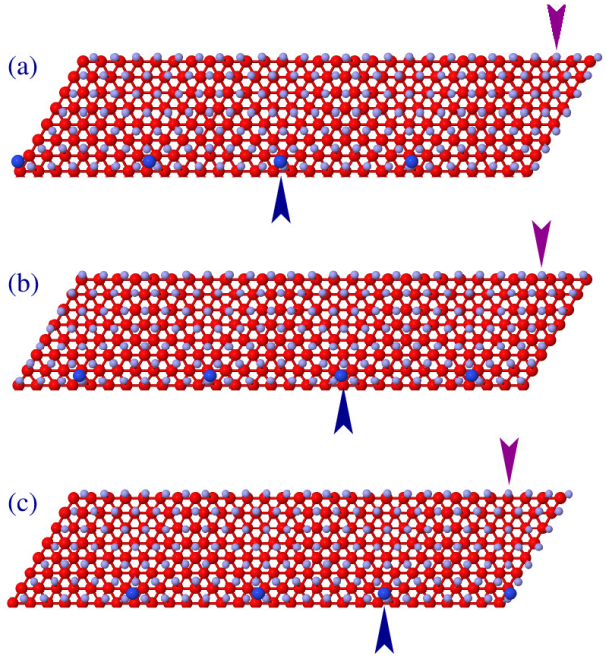


Figure 9: (Color online) A portion of three successive snapshots of the steady state of an underdense lubricant layer ($r_{\rm b} = 25/29$) forming a Moiré pattern, with $\Theta = 1$ antisoliton every top-layer line (same atomic symbol convention as in previous figures). Arrows track two atoms to help visualizing the leftward motion of the lubricant induced by a rightward motion of the top layer. Between snapshots (b) and (c) the leftmost line of lubricant particles has been remapped back inside the cell at its right side by the PBC.

amplitude are related to the necessity of a coordination of the forward motion with a transverse motion, induced by the tendency of the lubricant to follow the grooves of the bottom substrate, and detected as a nonzero average of the transverse velocity component, Fig. 8b. We explored different rotation angles $\alpha$. For comparatively small $|\alpha| \lesssim 15°$ and small $v_{\rm ext}$, a similar transverse motion establishes, characterized by periodic oscillations of the center-mass speed; for larger (nontrivial) $\alpha$ and for intermediate driving speed little or no substrate channeling nor net transverse motion arises, with the result that the center-mass motion is apparently non periodic (or of extremely long period). This is due to the advancing lubricant layer exploring the bottom-layer corrugation in an ever renewed mutual configuration. Importantly, in all tested cases, $w$ fluctuates (periodically or nonperiodically) around $w_{\rm quant}$, as long as $v_{\rm ext}$ is not too large.

### C. Dragging antisolitons: backward lubricant motion

A peculiar reversed lubricant dragging occurs when the lubricant is less dense than the bottom layer, i.e. $r_{\rm b} < 1$. Lines of dilation (antisolitons) are separated by in-register regions, as shown in Fig. 9. These antisoliton lines are soft defects with an enhanced mobility similar to that of the solitons of overdense layers: They can therefore be dragged rightward by the advancing top slider. Since these rightward traveling antisoliton lines are basically lines of missing atoms, or vacancies, the involved atoms, and thus the overall lubricant center of mass, move leftward, opposite to the driving $v_{\rm ext}$. As illustrated by the sequence of Fig. 9, a net backward lubricant motion ($v_{\rm c.m.} < 0$) is indeed observed. This result is perfectly accounted for by Eq. (18), which yields negative $a_{\rm sol}$, and by Eq. (24), which yields negative $w_{\rm quant}$.

The detailed example of this antisoliton case shown in Fig. 9 has $r_{\rm b} = 25/29$, so that the mismatch generates 4 antisoliton lines every 25 lubricant lattice spacings. We consider a top slider with $r_{\rm t} = 25/4$, to full commensuration with the antisoliton lattice, i.e. $\Theta = 1$. As reported in Fig 10, after the usual transient, simulations do show a net negative lubricant velocity oscillating around $v_{\rm c.m.\,x}/v_{\rm ext} = -0.16$, matching the predicted $w_{\rm quant} = -4/25$.

### D. Ar on graphite and other possible experimental realizations

The experimentally accessible configuration of Ar layers interposed as a lubricant in between a graphite substrate and a suitably nano-patterned top layer is a promising system where an antisoliton dragging can occur. The Ar monolayer is well know to be incommensurate to the graphite substrate[25], thus its soliton pattern

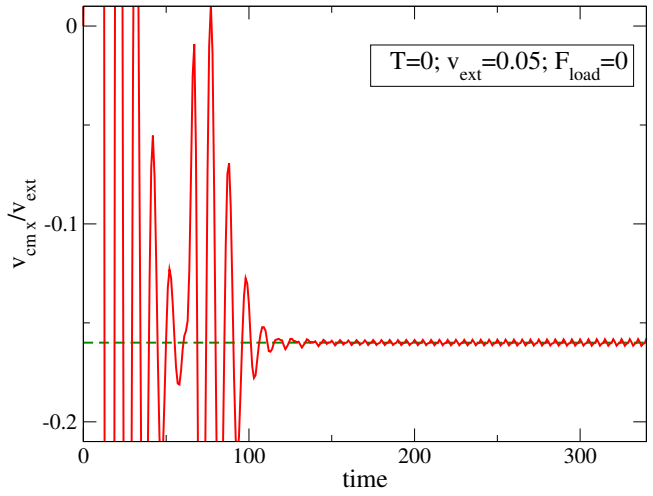


Figure 10: (Color online) The normalized average lubricant velocity, $w = v_{\mathrm{c.m.}\,x}/v_{\mathrm{ext}}$ as a function of time for the antisoliton geometry represented in Fig. 9, with $a_{\mathrm{t}} = 29/4 = 7.25$, $a_{\mathrm{p}} = 29/25 = 1.16$, $a_{\mathrm{b}} = 1$ for the top, lubricant and bottom layers corresponding to $r_{\mathrm{b}} = 25/29 = 0.86$. After an initial transient, $w$ starts to fluctuate around the negative value predicted by Eq. (24): $w_{\mathrm{quant}} = -4/25 = -0.160$, marked by the horizontal dashed line. The simulation is carried out for $N_{\mathrm{layer}} = 1$, $v_{\mathrm{ext}} = 0.05$, $F_{\mathrm{load}} = 0$, and $T = 0$.

is likely mobile.

To verify this possibility, we simulate this system by adopting the LJ parameters of the most basic model proposed in Ref. 26. The main difference with the hiterto studied model is that the bottom substrate is a honeycomb net, see Fig. 11, rather than the triangular lattice. For mechanical units we take the graphite in-plane lattice spacing $a_{\mathrm{b}} = a_{\mathrm{graphite}} = 246.4$ pm, $m = m_{\mathrm{Ar}} = 6.63 \times 10^{-26}$ kg, and $\varepsilon_{\mathrm{pp}} = \varepsilon_{\mathrm{Ar-Ar}} = 10.3$ meV. The Ar-C interaction energy $\varepsilon_{\mathrm{bp}} = \varepsilon_{\mathrm{Ar-C}} = 5.65$ meV $= 0.549\,\varepsilon_{\mathrm{Ar-Ar}}$[26]. We approximate the Ar lattice constant to $a_{\mathrm{Ar}} \simeq 20/13\,a_{\mathrm{graphite}} \simeq 379$ pm. For the top substrate we assume a triangular nanopattern with $a_{\mathrm{t}} = 20/7\,a_{\mathrm{graphite}} \simeq 704$ pm, such to produce a coverage $\Theta = 1$. For the $\sigma_{\mathrm{tp}}$ and $\epsilon_{\mathrm{tp}}$ parameters we adopt tentatively the Ar-C ones[26].

Even at the comparably large simulated speed $v_{\mathrm{ext}} = 0.05\,m^{-1/2}\varepsilon_{\mathrm{pp}}^{1/2} = 7.9$ m/s (see Table I), we do find quantized antisoliton motion, with the lubricant running backward, precisely at the speed $v_{\mathrm{c.m.}}/v_{\mathrm{ext}} = w_{\mathrm{quant}} = -7/13 \simeq -0.538$ predicted by Eq. (24). We verified that the quantized state is retrieved also in the following conditions: (i) Ar bilayer ($N_{\mathrm{layer}} = 2$), rather than monolayer, (ii) the application of $F_{\mathrm{load}} = 0.004$, representing a 1 MPa load, and (iii) a looser nanopattern of the top layer, namely $a_{\mathrm{t}} = 40/7\,a_{\mathrm{graphite}} \simeq 1408$ pm, i.e. $\Theta = 2$. However, we could retrieve no quantized state for other (non-integer) coverages, at least at the driving speeds we tested. We conclude therefore that the Ar/graphite system is potentially suitable for the observation of antisoliton dragging, with a remarkable backward lubricant motion, provided a nanopatterned top layer of a properly tuned periodicity can be assembled and brought into contact with the Ar layer.

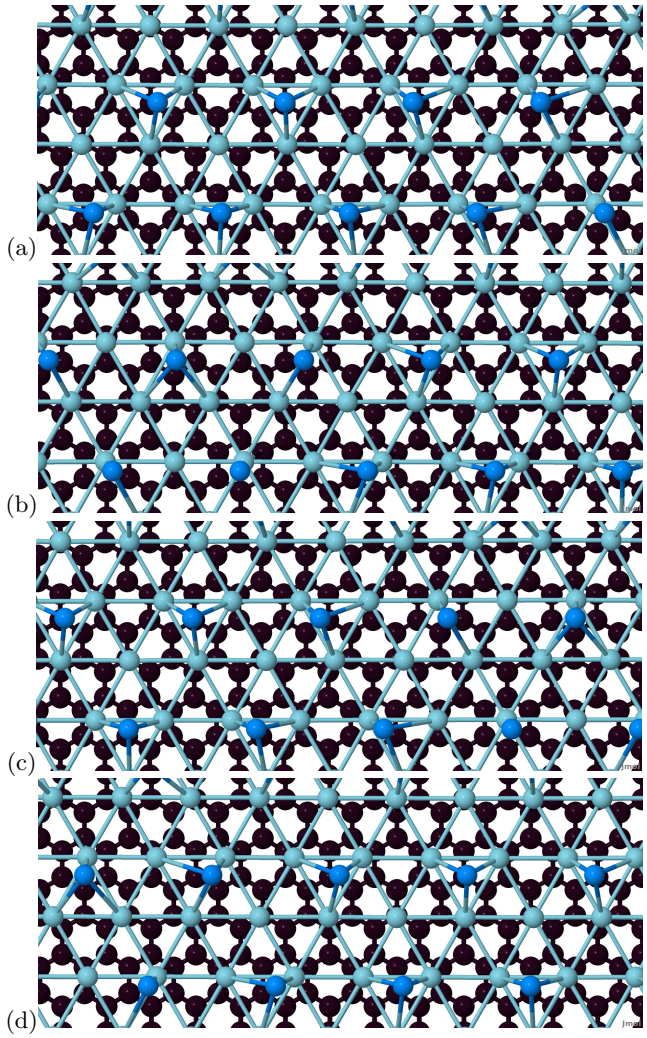


Figure 11: (Color online) Successive snapshots of the "quantized" sliding state of an Ar (light-blue/clear) monolayer confined between a static graphite layer (black), and a nanopatterned top layer (dark blue) advancing rightward at a speed $v_{\mathrm{ext}} = 7.9$ m/s. The time interval between successive frames is 12.5 ps. The top layer lattice spacing $a_{\mathrm{t}} \simeq 0.7$ nm, corresponds to coverage $\Theta = 1$ of the antisoliton pattern. The leftward motion of the Ar layer is evident.

Analogous incommensurate configurations occur for other noble gases on metal surfaces such as Ag(111) and Pb(111). It is quite possible that similar quantized sliding regimes occur in such systems as well. However, in some cases the noble gas-metal interaction may be comparably stronger[27] than with graphite, possibly resulting in a higher corrugation and practically pinned (anti)solitons.

An experimentally promising geometry which could reveal the quantized sliding phenomenology could be realized in surface force apparatus (SFA) experiments[28]

where atomically thin lubricant layers are confined between molecularly smooth mica surfaces. At a larger (meso) scale, the same mechanism could be realized by some modification of the setup used in Ref. 29 where a 2D crystal of colloidal particles is dragged by a flow of solvent over a periodic corrugation generated by a light interference pattern. A pattern or solitons or antisolitons, very similar to that illustrated for an atomic overlayer in Fig. 3, can form and slide around when the two lattice spacings do not match[30]. In this case, a second independent periodic interference pattern might be used to mimic the sliding top layer and drag the soliton pattern along. At an even larger (macro) scale, friction experiments with a 2D "granular" system consisting of photoelastic disks confined in a channel[31] might be considered with channel walls formed by two corrugated and vertically oriented Plexiglas sheet, once again reproposing the soliton mechanisms under shear.

### E. The velocity plateau

Quantized sliding, where the ratio $v_{\mathrm{c.m.}\,x}/v_{\mathrm{ext}}$ remains constant, forming a flat "plateau", as a function of parameters, occurs within certain ranges of physical conditions, speed, etc. Of course, plateaus do not extend to arbitrary values of the physical parameters, but end at certain boundaries marking a sort of "dynamical phase diagram". The point in parameter space where the quantized sliding terminates identifies a sort of dynamical depinning transition, where the top slider's grip on solitons is lost.[9]. A variation of system parameters will generally affect the plateau extension and the precise occurrence of this dynamic depinning.

The most straightforward way to end the quantized sliding state is by increasing the driving velocity $v_{\mathrm{ext}}$. Indeed, simulations show that, once the plateau exists for a given speed $v_{\mathrm{ext}}$, the quantized state holds for all smaller speeds, at least at zero or low enough temperature. In contrast, for increasing $v_{\mathrm{ext}}$, beyond a critical speed $v_{\mathrm{crit}}$ the quantized state is generally lost. The reason for the existence of such a maximum speed is that the quantized state is based on the forced advancement of a soliton deformation at speed $v_{\mathrm{ext}}$ along the lubricant crystal. As soon as $v_{\mathrm{ext}}$ is larger than the lubricant speed of sound, the amplitude of this soliton wave decays rapidly due to inertia, until it disappears together with the quantized state. However, whenever the pinning between the soliton pattern and the top substrate is weak, the depinning may occur earlier, for smaller $v_{\mathrm{ext}}$. It is then natural to regard the critical speed $v_{\mathrm{crit}}$ as a measure of the robustness of the quantized state. We map this robustness under variations of other parameters: temperature $T$, the load $F_{\mathrm{load}}$ per particle in the top layer, the soliton coverage ratio $\Theta$, and the number of lubricant layers $N_{\mathrm{layer}}$.

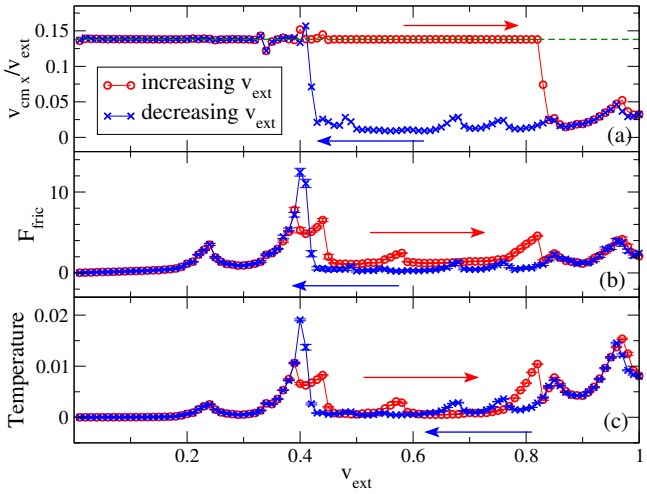


Figure 12: (Color online) The plateau of the dynamically pinned state and its tribological properties, for the model described in Fig. 3. As a function of the adiabatically increased (circles) or decreased (squares) top-layer velocity $v_{\mathrm{ext}}$, the panels report: (a) the average velocity ratio $w = v_{\mathrm{c.m.}\,x}/v_{\mathrm{ext}}$ compared to the plateau value $w_{\mathrm{quant}} = 4/29 \simeq 0.1379$, Eq. (24), dashed line; (b) the average friction force experienced by the top layer; and (c) the average lubricant kinetic energy per particle relative to the lubricant center of mass.

#### 1. *The quantized state as a function of the driving velocity*

We use sequences of linked MD simulations to investigate the termination of the quantized-sliding state, as $v_{\mathrm{ext}}$ is changed in small steps. A similar study was carried out for the 1D Frenkel-Kontorova model[32] and for the 1D and 2D analogous of the present sliding model[4,5,8], where a hysteretic termination of the plateau was identified in underdamped dynamics. As $v_{\mathrm{ext}}$ is increased adiabatically, coming from the low-speed quantized state, there is a good chance that the ensuing sliding state remains quantized. This quantized sliding will therefore generate a plateau of constant $w = v_{\mathrm{c.m.}\,x}/v_{\mathrm{ext}}$, extending until a critical speed $v_{\mathrm{crit}}$, where the pinning of solitons to the top slider corrugation loses its battle against the dissipative forces acting on the lubricant layer, represented by Eq. (8). For $v_{\mathrm{ext}} \geq v_{\mathrm{crit}}$, a non-quantized state ensues, characterized by an irregular lubricant motion, and a center-mass speed fluctuating non periodically far from the quantized value $w_{\mathrm{quant}} v_{\mathrm{ext}}$. Upon adiabatic decreasing $v_{\mathrm{ext}}$ from this high-speed non-quantized state, the quantized state is usually recovered at a speed lower than the depinning $v_{\mathrm{crit}}$, a clearly hysteretic unpinning-pinning dynamical transition. In the intermediate range, the velocity ratio $w = v_{\mathrm{c.m.}\,x}/v_{\mathrm{ext}}$ is therefore a multivalued function of $v_{\mathrm{ext}}$.

Figure 12a illustrates this hysteretic depinning for the fully-commensurate $\Theta = 1$ model of Fig. 3, with $F_{\mathrm{load}} = 0$ and $T = 0$. The precise value of $v_{\mathrm{crit}}$ is obtained by ramping $v_{\mathrm{ext}}$ up in small steps; at every step the integration starts from the final configuration of the

preceding step. For these model parameters, we estimate $v_{\rm crit} = 0.825 \pm 0.005$. Following the same procedure with downward steps to locate the speed of recovery of the quantized state, we obtain $v_{\rm crit\,down} = 0.415 \pm 0.005$.

The hysteretic loop is due to the "dynamically metastable" nature of the dynamically pinned state. The finite simulation time $t_{\rm calc}$ and the absence of thermal fluctuations ($T = 0$) can leave the system locked in a dynamically unfavorable state, which survives until the system jumps into the appropriate dynamically favored state.

The friction force reported in Fig. 12b, exhibits a non-trivial structure. Around $v_{\rm ext} \simeq 0.24$, 0.39, 0.44, 0.58, and 0.82, the friction force (and consequently the dissipated power) is seen to peak and then drop to a smaller value. These friction peaks arise at the resonances of the "washboard" frequency of the advancing lubricant crystal with the bottom lattice with specific vibrational normal modes of the lubricant lattice. The resonance are reflected by peaks in the lubricant internal kinetic energy, see Fig. 12c. Across these resonant peaks, the value of $w$ remains mostly stable, except at the last of these transitions, marking the end of the quantized plateau, with $w$ moving away from the $w_{\rm quant}$ value, again coinciding with a significant drop in friction. At resonant peaks rearrangements of the pinned configuration may occur, with the top layer displacing to grab and drag the soliton pattern to a different mutual arrangement, always guaranteeing the regular advancement of the solitons/antisolitons realizing the dynamically pinned state and the associated quantized velocity.

A similar phenomenon is observed on the way back, decreasing $v_{\rm ext}$: The friction force and the lubricant internal kinetic energy undergo several small jumps corresponding to washboard resonances related to the top-layer advancement over the non-quantized quasi-static state. Corresponding to the resonances also $v_{{\rm c.m.}\,x}$ has small bumps, until eventually the plateau state is recovered, with a sudden jump in the friction force. The hysteretic depinning regime observed in the present fully 3D model is therefore richer than that observed in the purely 1D model[10] or in the 1+1D model of Refs. 11,12.

If the ideal one-to-one geometrical interlocking between the top corrugation and the lubricant soliton pattern ($a_{\rm t} = a_{\rm sol}$, i.e. $\Theta = 1$) is of course an especially favorable condition for the occurrence of dynamical pinning, we do find velocity quantization even for $\Theta \neq 1$, although not for all investigated values of $\Theta$. Assuming that the previously unraveled 1D mapping to the Frenkel-Kontorova model[9] is also meaningful in the present richer interface geometry, the coverage ratio should thus affect the robustness of the velocity plateau. Indeed, simulations with simple integer ratios, such as $\Theta = 2$ and $\Theta = 1/2$, do show quantized sliding essentially equivalent to the case with $\Theta = 1$. Other configurations with fractional $\Theta$, where the top-lattice crystal lines turn to be more pronouncedly out-of-registry with the lubricant soliton pattern, give rise to a weakening, or even the loss,

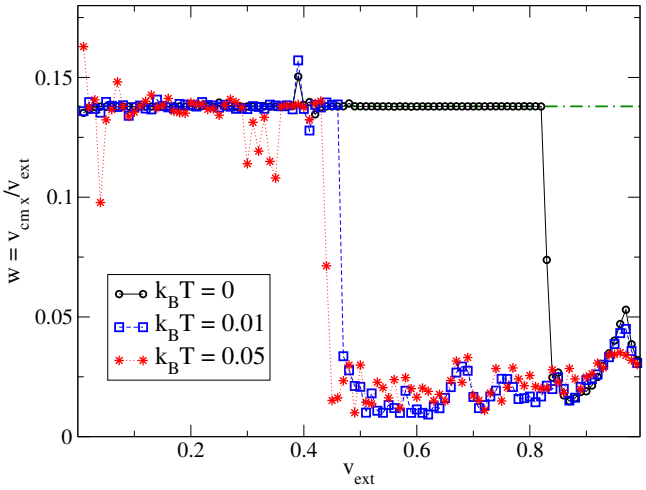


Figure 13: (Color online) The effect of temperature on the plateau of the dynamically pinned state studied for increasing $v_{\rm ext}$. The circles are the same $T = 0$ data as in Fig. 12a. Each square or star is obtained as by averaging $v_{{\rm c.m.}\,x}$ over the last 70% of an at least 100 time units long Langevin simulation at finite temperature, started from the final state of the previous configuration. The dot-dashed line marks the plateau value $w_{\rm quant} = 4/29$ for the considered geometry.

of the quantized plateau.

By following the quantized plateau up to its critical speed for several values of the mismatch ratio $r_{\rm b} = a_{\rm b}/a_{\rm p}$, ranging from solitonic ($r_{\rm b} > 1$) to antisolitonic ($r_{\rm b} < 1$), we find a rather erratic dependence of $v_{\rm crit}$ on $r_{\rm b}$. In this case, the different degree of efficiency of the grip on solitons and thus of robustness of the quantized dynamics, may be partially related to random initial conditions, hardly a controllable element.

### 2. *Effects of temperature*

To investigate the robustness of the quantized state against thermal fluctuations, we run finite-temperature simulations in the same conditions as the zero-temperature runs discussed until now. The results are summarized in Fig. 13. For low temperature $k_{\rm B}T = 0.0001$ and 0.001 (not shown), even though the trajectories of individual particles are affected by thermal fluctuations, $w$ exhibits no significant deviation from $T = 0$.

For larger $k_{\rm B}T = 0.01$ and 0.05 we observe deviations and fluctuations around the quantized plateau speed, see Fig. 13. Similar deviations were found in the 1+1D model[11,12]. Notice that these deviations in $w$ reflect very wide instantaneous fluctuations, often far exceeding the average lubricant velocity. The averaging over a finite simulation duration $t_{\rm calc}$ integrates out these large fluctuations, suggesting that, over an appropriately reduced range of $v_{\rm ext}$, the system fluctuates around the quantized sliding state, which still dictates the average lubricant advancement speed. If longer simulations were

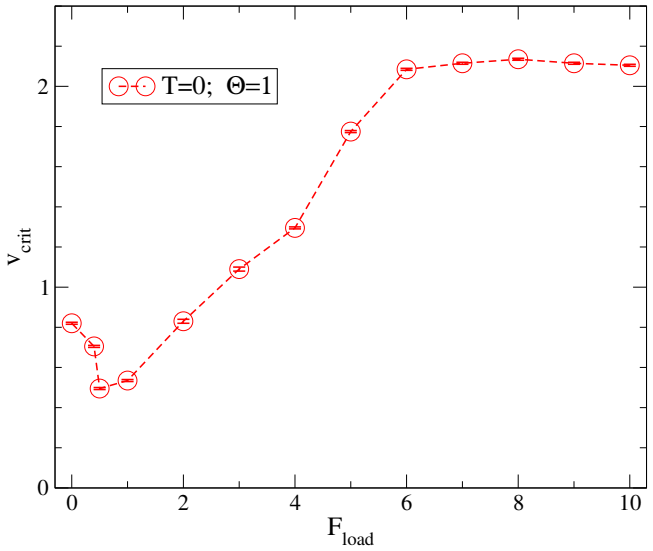


Figure 14: (Color online) The depinning speed $v_{\rm crit}$ as a function of the applied load per particle $F_{\rm load}$ for the same model as in Fig. 3. Beyond the small-load region, the quantized-sliding state exhibits an overall benefit of increased load.

carried out, further averaging would decrease the fluctuation amplitude, thus indicating that the thermal regime is indeed randomly fluctuating around the dynamically pinned state. In temperature, the dynamical depinning tends to occur at a generally smaller driving speed.

For even larger $k_{\rm B}T = 0.1$, the tendency to in-plane thermal expansion of the lubricant layer, frustrated by the in-plane PBC, resolves in the expulsion of a small fraction of atoms from the lubricant layer, which thus gets rid of the soliton-originating mismatch to the bottom layer. As a result, the quantized sliding state is completely absent at such high temperature.

### 3. *Effects of applied load*

We also investigate the effect of changing the load applied between the sliders, squeezing the lubricant layer among them. The lubricant in turn is not perfectly flat, because in-register regions are composed by hollow-site atoms, which move closer to the bottom slider, while the soliton regions consist of atoms occupying bridge or top sites, which are therefore pushed upward. In matched ($\Theta = 1$) configurations and in the ensuing quantized sliding state, the top slider atoms tend to catch over the in-register regions which are the most vertically depressed lubricant areas, rather than over the solitons, where the lubricant is sticking out locally. As a result, the applied load squeezes down onto the in-register regions, and affects the solitonic regions more marginally. Thus, the increased load should make it more difficult for the soliton pattern to unpin itself from the top-layer corrugation.

To investigate the load dependence of the quantized plateaus we consider several $F_{\rm load}$ values, and for each

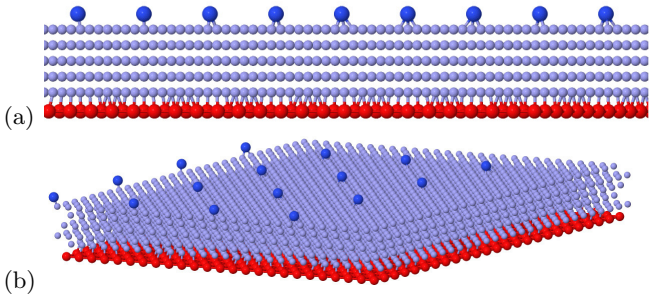


Figure 15: (Color online) (a) Side and (b) perspective view of a $N_{\rm layer} = 5$ lubricant layers model, with the same lattice mismatch and other parameters as in Fig. 3.

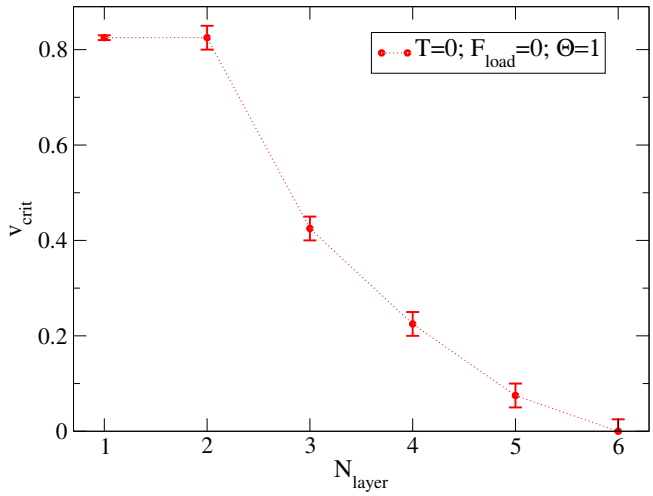


Figure 16: (Color online) The depinning speed $v_{\rm crit}$ as a function of $N_{\rm layer}$ for a multilayer configuration of the type illustrated by Fig. 15, with the same simulation parameters as in Fig. 3. The quantized sliding state weakens for increasing number of lubricant layers $N_{\rm layer} \geq 2$.

of them we cycle $v_{\rm ext}$ up in small steps, as described in Sect. III E 1, to determine $v_{\rm crit}$. We collect the resulting values of $v_{\rm crit}$ for varied load in Fig. 14, which shows that, by increasing $F_{\rm load}$, $v_{\rm crit}$ generally rises, thus indicating that, as expected, the quantized state is extended under a larger load $F_{\rm load}$.

### 4. *Multiple lubricant layers*

In boundary lubrication, the lubricant as a rule solidifies into a multiplicity of layers, whose thickness is gradually reduced by squeeze-out under pressure, until a single layer is just an extreme possibility. It is therefore important to verify whether the plateau dynamics is an exclusive prerogative of the single lubricant layer studied so far, or whether it will occur even for multilayer solid lubricant films – although of course with generally smaller and less robust plateaus. Figure 15 displays the typical arrangement of lubricant particles relative to the

substrates in a lubricant multi-layer configuration. Soliton deformation affect mostly the lubricant layer in direct contact with the bottom substrate. The atoms of the uppermost lubricant layer are spaced almost regularly, but the residual vertical displacements can be sufficient for the soliton pattern to ingrain in the top substrate.

For multiple lubricant layers (up to $N_{\rm layer} = 5$), we recover quantized velocity plateaus, for the case examined of full matching $\Theta = 1$, with $F_{\rm load} = 0$ and $T = 0$. We evaluate the robustness of the quantized sliding state by determining the critical speed $v_{\rm crit}$ where the quantized plateau ends in this multilayer lubricant case. Figure 16 shows that the broadest plateau is achieved for $N_{\rm layer} = 1$. Its width is still as large at $N_{\rm layer} = 2$; further lubricant thickening reduces $v_{\rm crit}$ progressively. This decrease is not surprising, as the power-law weakening of soliton-induced corrugation across the film makes the grip on solitons by the top slider harder and harder for thicker and thicker layers. For $N_{\rm layer} > 5$, we could detect no quantized-sliding dynamics, even at very small $v_{\rm ext}$.

## IV. DISCUSSION AND CONCLUSION

We present a simulation study of the relative sliding of rigid incommensurate crystal surfaces separated by a 3D solid and fully mobile lubricant film, whose interatomic interactions were assumed to be of LJ type. The "quantization" of the lubricant's sliding speed previously uncovered in much more idealized, lower dimensional models is fully confirmed in this more realistic case. The quantized relative speed plateau as a function of overall sliding speed is detected very clearly and demonstrated to extend over broad parameters ranges including applied load, number of lubricant layers and commensuration ratio between the top layer and the soliton lattice.

Focusing mainly on unrotated lattices and a single lubricant layer, we find perfect plateaus at the same geometrically determined velocity ratio $w_{\rm quant}$ as observed in the 1D and 2D models, both in case of solitons (forward lubricant sliding) and of antisolitons (backward soliton sliding). We find that the soliton pinning to the top slider leading to plateau quantization is abandoned by increasing the sliding velocity $v_{\rm ext}$ above a critical value $v_{\rm crit}$. It is eventually retrieved when $v_{\rm ext}$ is reduced back down to $v_{\rm crit\,down} < v_{\rm crit}$, thus with a hysteresis. The quantized sliding state is strengthened by an applied load. Although the optimal rate of commensuration for quantization to occur is perfect 1:1 matching ($\Theta = 1$) between soliton lattice and top slider lattice of kinks to the upper slider lattice, weaker but definite quantized regimes exist even for $\Theta \neq 1$ .

In the attempt to address slightly more realistic conditions, we also model a multilayer as opposed to monolayer LJ solid lubricant; and a monolayer and a bilayer of solid Ar acting as a lubricant between a flat graphite surface and a nanopatterned slider. Quantized sliding is recovered in both cases, although in a rather fragile form for $N_{\rm layer} > 3$. We see no reason for the same Moiré-pattern dragging mechanism to be restricted to LJ systems: It is likely to show up in many sliding-friction experiments, as long as a crystalline lubricant thin film (e.g. a graphene layer) is sandwiched in between two different lattice-mismatched crystalline sliders.

The present preliminary investigation of thermal effects confirms the robustness of the quantized state. Like for the 1+1D model of Refs. 11,12, we find that (i) the quantized plateau becomes noisy, with the relative lubricant velocity $w$ fluctuating around $w_{\rm quant}$, (ii) the dynamical depinning, rather than a sharp hysteretic transition, behaves as a continuous crossover, and (iii) this crossover occurs at a generally smaller speed $v_{\rm ext}$. A further systematic investigation of thermal effects and of the mutual rotation of the three crystalline layers promises nontrivial developments.

### Acknowledgments

We acknowledge useful discussion with P. Ballone and I.E. Castelli. This work was partly supported by ERC Advanced Research Grant N. 320796 MODPHYSFRICT, by MIUR, through PRIN-2010LLKJBX-001, by SNSF, through SINERGIA Project CRSII2 136287/1, by COST Action MP1303, and by the EU-Japan Project LEMSUPER.

[1] A. Vanossi, N. Manini, M, Urbakh, S. Zapperi, and E. Tosatti, Rev. Mod. Phys. **85**, 529 (2013).
[2] A. Vanossi, N. Manini, G. Divitini, G. E. Santoro, and E. Tosatti, Phys. Rev. Lett. **97**, 056101 (2006).
[3] G. E. Santoro, A. Vanossi, N. Manini, G. Divitini, and E. Tosatti, Surf. Sci. **600**, 2726 (2006).
[4] M. Cesaratto, N. Manini, A. Vanossi, E. Tosatti, and G. E. Santoro, Surf. Sci. **601**, 3682 (2007).
[5] A. Vanossi, G. E. Santoro, N. Manini, M. Cesaratto, and E. Tosatti, Surf. Sci. **601**, 3670 (2007).
[6] N. Manini, M. Cesaratto, G. E. Santoro, E. Tosatti, and A. Vanossi, J. Phys.: Condens. Matter **19**, 305016 (2007).
[7] A. Vanossi, G. E. Santoro, N. Manini, E. Tosatti, and O. M. Braun, Tribol. Int. **41**, 920 (2008).
[8] N. Manini, A. Vanossi, G. E. Santoro, and E. Tosatti, Phys. Rev. E **76**, 046603 (2007).
[9] A. Vanossi, N. Manini, F. Caruso, G. E. Santoro, and E. Tosatti, Phys. Rev. Lett. **99**, 206101 (2007).
[10] N. Manini, G. E. Santoro, E. Tosatti, and A. Vanossi, J. Phys.: Condens. Matter **20**, 224020 (2008).
[11] I. E. Castelli, R. Capozza, A. Vanossi, G. E. Santoro, N. Manini, and E. Tosatti, J. Chem. Phys. **131**, 174711

(2009).
[12] I. E. Castelli, N. Manini, R. Capozza, A. Vanossi, G. E. Santoro, and E. Tosatti, J. Phys.: Condens. Matter **20**, 354005 (2008).
[13] A. D. Novaco and J. P. McTague, Phys. Rev. Lett. **38**, 1286 (1977).
[14] We adopt a fairly small value $\eta = 0.05$ (in model units $a_{\rm b}^{-1}\,\varepsilon_{\rm pp}^{1/2}\,m^{1/2}$), leading to clearly underdamped atomic dynamics, with a modest influence of the thermostat on the lubricant motion.
[15] O. M. Braun and M. Peyrard, Phys. Rev. E **63**, 046110 (2001).
[16] O. M. Braun and A. G. Naumovets, Surf. Sci. Rep. **60**, 79 (2006).
[17] L. Kantorovich, Phys. Rev. B **78**, 094304 (2008).
[18] L. Kantorovich and N. Rompotis, Phys. Rev. B **78**, 094305 (2008).
[19] O. M. Braun, N. Manini, and E. Tosatti, Phys. Rev. B **78**, 195402 (2008).
[20] A. Benassi, A. Vanossi, G. E. Santoro, and E. Tosatti, Phys. Rev. B **82**, 081401 (2010).
[21] O. M. Braun and N. Manini, Phys. Rev. E **83**, 021601 (2011).
[22] A. Benassi, A. Vanossi, G. E. Santoro, and E. Tosatti, Tribol. Lett. **48**, 41 (2012).
[23] M. P. Allen and D. J. Tildesley, *Computer Simulations of Liquids* (Oxford University Press, Oxford, 1991).
[24] O. M. Braun and Yu. S. Kivshar, *The Frenkel-Kontorova Model: Concepts, Methods, and Applications* (Springer, Berlin, 2004).
[25] L. W. Bruch, R. D. Diehl, and J. A. Venables, Rev. Mod. Phys. **79**, 1381 (2007).
[26] S. R. Sharma, S. F. O'Shea, and W. J. Meath, Phys. Rev. B **40**, 6356 (1989).
[27] J. Lv, M. Bai, W. Cui, and X. Li, Nanoscale Res. Lett. **6**, 200 (2011).
[28] J. N. Israelachvili, Surf. Sci. Rep. **14**, 109 (1992).
[29] T. Bohlein, J. Mikhael, and C. Bechinger, Nat. Mater. **11**, 126 (2012).
[30] A. Vanossi, N. Manini, and E. Tosatti, P. Natl. Acad. Sci. USA **109**, 16429 (2012).
[31] J. Krim, P. Yu, and R. P. Behringer, Pure Appl. Geophys. **168**, 2259 (2011).
[32] A. Vanossi, G. Santoro, and V. Bortolani, J. Phys.: Condens. Matter **16**, S2895 (2004).